ELSEVIER

NeuroImage

www.elsevier.com/locate/ynimg
NeuroImage 24 (2005) 50–60

ICA-based procedures for removing ballistocardiogram artifacts from EEG data acquired in the MRI scanner

G. Srivastava,[a,b] S. Crottaz-Herbette,[a] K.M. Lau,[a] G.H. Glover,[c] and V. Menon[a,d,e,*]

[a]*Department of Psychiatry and Behavioral Sciences, Stanford University, Stanford, CA 94305, USA*
[b]*Department of Electrical Engineering, Stanford University, Stanford, CA 94305, USA*
[c]*Department of Radiology, Stanford University, Stanford, CA 94305, USA*
[d]*Program in Neuroscience, Stanford University, Stanford, CA 94305, USA*
[e]*Stanford Brain Research Institute, Stanford University, Stanford, CA 94305, USA*

Received 23 December 2003; revised 29 July 2004; accepted 28 September 2004

Electroencephalogram (EEG) data acquired in the MRI scanner contains significant artifacts, one of the most prominent of which is ballistocardiogram (BCG) artifact. BCG artifacts are generated by movement of EEG electrodes inside the magnetic field due to pulsatile changes in blood flow tied to the cardiac cycle. Independent Component Analysis (ICA) is a statistical algorithm that is useful for removing artifacts that are linearly and independently mixed with signals of interest. Here, we demonstrate and validate the usefulness of ICA in removing BCG artifacts from EEG data acquired in the MRI scanner. In accordance with our hypothesis that BCG artifacts are physiologically independent from EEG, it was found that ICA consistently resulted in five to six independent components representing the BCG artifact. Following removal of these components, a significant reduction in spectral power at frequencies associated with the BCG artifact was observed. We also show that our ICA-based procedures perform significantly better than noise-cancellation methods that rely on estimation and subtraction of averaged artifact waveforms from the recorded EEG. Additionally, the proposed ICA-based method has the advantage that it is useful in situations where ECG reference signals are corrupted or not available.

Keywords: Simultaneous EEG/fMRI; Ballistocardiogram artifact; Independent Component Analysis; Spectral Power Comparison

Introduction

Combining information from EEG and fMRI holds great promise for examining the spatial and temporal dynamics of sensory and cognitive processes underlying brain function (Ahlfors et al., 1999; Babiloni et al., 2000a,b; Dale et al., 2000; George et al., 1995; Menon et al., 1997; Woldorff et al., 1999). Concurrent acquisition of EEG and fMRI has proven to be challenging for a number of reasons including safety and data quality (Goldman et al., 2000). In the past 5 years, several brain imaging centers have developed and refined techniques for simultaneous acquisition of EEG and fMRI data (Bonmassar et al., 2001; Krakow et al., 2000; Lemieux et al., 2001; Salek-Haddadi et al., 2002) and have used them to detect EEG spikes, characterize resting state EEG and fMRI, and study event-related potentials (ERPs) (Bonmassar et al., 1999; Liebenthal et al., 2003). Common to all these studies is the problem of removing BCG artifacts which contaminate EEG data in the scanner (Allen et al., 1998; Bonmassar et al., 2002; Sijbers et al., 2000). In this paper, we demonstrate the application of ICA-based procedures to remove BCG artifacts from simultaneous EEG data recorded in the MRI scanner. We show that ICA-based procedures can significantly reduce the spectral power associated with BCG artifacts and that the performance of these procedures is superior to BCG artifact removal techniques that rely on averaged artifact subtraction (Allen et al., 1998; Goldman et al., 2000).BCG artifacts are a consequence of electromotive force produced on the EEG electrodes due to small head movements, such as those caused by cardiac pulsation, inside the scanner magnetic field. As pointed by Sijbers et al. (2000), there are three major sources of BCG artifacts: (1) small but firm movement of the electrodes and the scalp due to expansion and contraction of scalp arteries between systolic and diastolic phase, (2) fluctuation of the Hall-voltage due to the pulsatile changes of the blood in the arteries, and (3) small cardiac related movements of the body. The cardiac pulse generates artifacts with amplitudes considerably larger than EEG signal fluctuations. It is therefore important to develop methods to identify and remove these artifacts in a robust manner.

Most approaches for eliminating BCG artifacts to date have focused on either (1) Averaged Artifact Subtraction (AAS), in which a BCG artifact template is estimated by averaging over the intervals of EEG signal that are corrupted by the artifact and

* Corresponding author. Program in Neuroscience and Department of Psychiatry and Behavioral Sciences, 401 Quarry Road, Stanford University School of Medicine, Stanford, CA 94305-5719. Fax: +1 520 244 6474.
E-mail address: menon@stanford.edu (V. Menon).
Available online on ScienceDirect (www.sciencedirect.com.)

1053-8119/$ - see front matter © 2004 Elsevier Inc. All rights reserved.
doi:10.1016/j.neuroimage.2004.09.041

subsequent subtraction of the template from the corrupted segments to obtain clean signal (Allen et al., 1998) or (2) Adaptive filtering techniques, which make use of correlations between a reference ECG channel and the EEG channels to estimate the contribution of BCG artifact in the EEG signals which is then subtracted to give clean signals (Bonmassar et al., 2002).

The AAS procedure is the most commonly employed method for removing the BCG artifact from EEG data (Allen et al., 1998). In this procedure, the QRS peaks in the ECG signal are first detected and then EEG activity time-locked to these peaks is averaged to give an estimate of the pulse artifact. The average artifact is then subtracted from the EEG. Goldman et al. (2000) have used a method that is conceptually similar to AAS procedure, but it differs in the weights applied to data segments prior to averaging. These weights vary inversely with the temporal displacement from the current sample to compensate for the slow changes in the BCG artifact. Along similar lines, Sijbers et al. (2000) have used QRS onset detection for creating a template of the BCG artifact based on adaptive filtering. They point out that simple averaging would not lead to a satisfactory template, as the ECG is not a stationary signal and hence the rate and duration of BCG artifacts may vary over time. So in their approach, median filtering was performed for obtaining an artifact template because it adapts to changes in ECG signals over time. Bonmassar et al. (2002) used motion information recorded from a piezoelectric sensor placed on the temporal artery to estimate the motion artifact noise (mostly BCG), followed by adaptive filtering to subtract the artifact.

Automated AAS procedures are not amenable for removing BCG artifacts in the interleaved scanning scenario which is described in Materials and methods. In such a case, the duration of BCG artifacts may vary from trial to trial since some of the BCG artifacts lie partially in scanning and non-scanning intervals. These cannot be removed satisfactorily by AAS as it relies on the estimation of artifact template for the entire duration of the artifact. One apparent problem with the adaptive filtering approach is that it assumes that the reference signal contains only the activity of the source of noise and not other neural signals. This assumption may not be true if the reference signal is also acquired on or near the scalp because in that case, it will have contributions from other neural generators and the correlations between the reference signal and the EEG signal will give an erroneous estimate of noise. Using such methods might lead to removal of useful neurophysiological signals as well. Therefore, new procedures are required which can overcome the problem of variability in ECG pulse rate and duration, the need for an artifact template, and the need for a reference ECG channel. An ICA-based procedure provides a potential approach to circumvent these problems as it makes no assumptions about the morphology (rate or duration) of the mixing signals and does not necessitate the use of a reference signal for extracting BCG artifacts.

ICA can be used to recover independent sources from a set of simultaneously acquired signals that result from a linear mixing of the source signals (Comon, 1994). The ICA algorithm makes no assumption about the mixing process except that it is linear. A good intuitive mathematical formulation of ICA is given in Jung et al. (2001a,b).

A number of procedures have been developed in recent years to isolate the source signals (Hyvarinen et al., 2001); here, we identify independent components (ICs) using the infomax approach (Bell and Sejnowski, 1995; Lee et al., 1999).

ICA has been used successfully by Tong et al. (2001) to remove ECG interference from EEG recordings in small animals. Applied to human EEG data, ICA has been used to separate complex multichannel data into spatially fixed and temporally independent components without requiring detailed models of either the dynamics or the spatial structure of the separated components (Jung et al., 2001a,b). In recent years, ICA has become increasingly popular for artifact removal and characterizing distinct or overlapping brain or extra-brain sources of activations. It has been employed for analysis of single-trial event related potentials, for removal of blinks, eye movements, temporal muscle activity, and electrode artifacts (Iriarte et al., 2003; Jung et al., 2000a,b; 2001a,b).

Here, we apply ICA-based procedures for isolating and removing BCG artifacts from human EEG data acquired in the scanner. One weakness of previous studies in the field is that none of them have provided a quantitative comparison between

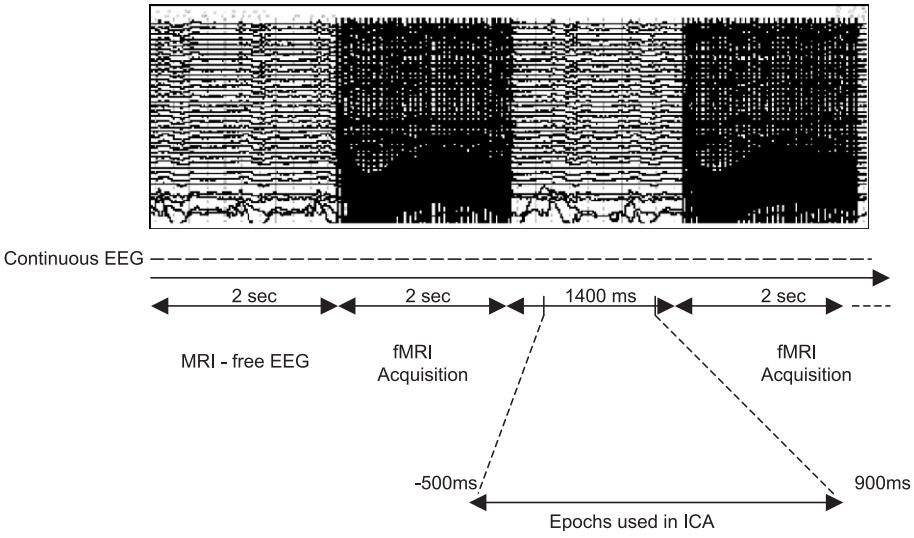

Fig. 1. Timing diagram of interleaved EEG/fMRI data acquisition. EEG data were acquired concurrently with clustered fMRI data acquisition. The duration of each fMRI acquisition was 2 s and it was followed by 2 s of MRI-free EEG. EEG epochs used in this study started 500 ms after the end of the fMRI acquisition, and had a duration of 1400 ms. This segment was free of MRI gradient artifacts.

procedures commonly used for removing BCG artifacts. In the absence of such a comparison, it is very difficult to assess the relative strengths of various approaches. Here, we provide quantitative evidence that our ICA-based procedures performs better than the more standard AAS-based procedures.

Materials and methods

Subjects

Five right-handed healthy volunteers (4 males and 1 female, ages 20–24 years) participated in this study. All study protocols were approved by the human subjects committee at Stanford University School of Medicine, and subjects provided written informed consent prior to participation in the study.

EEG-fMRI acquisition

The spiral-in/out fMRI sequence was adapted for interleaved EEG acquisition using a clustered procedure comprising 2 s of EEG acquisition without MRI scanning, followed by 2 s of fMRI data acquisition (Fig. 1). To maintain proper synchrony during the interleaved EEG and fMRI acquisition, each fMRI acquisition was triggered using the stimulation software (Eprime 1.1, Psychology Software Tools, Inc.) and trigger time was also stored in EEG

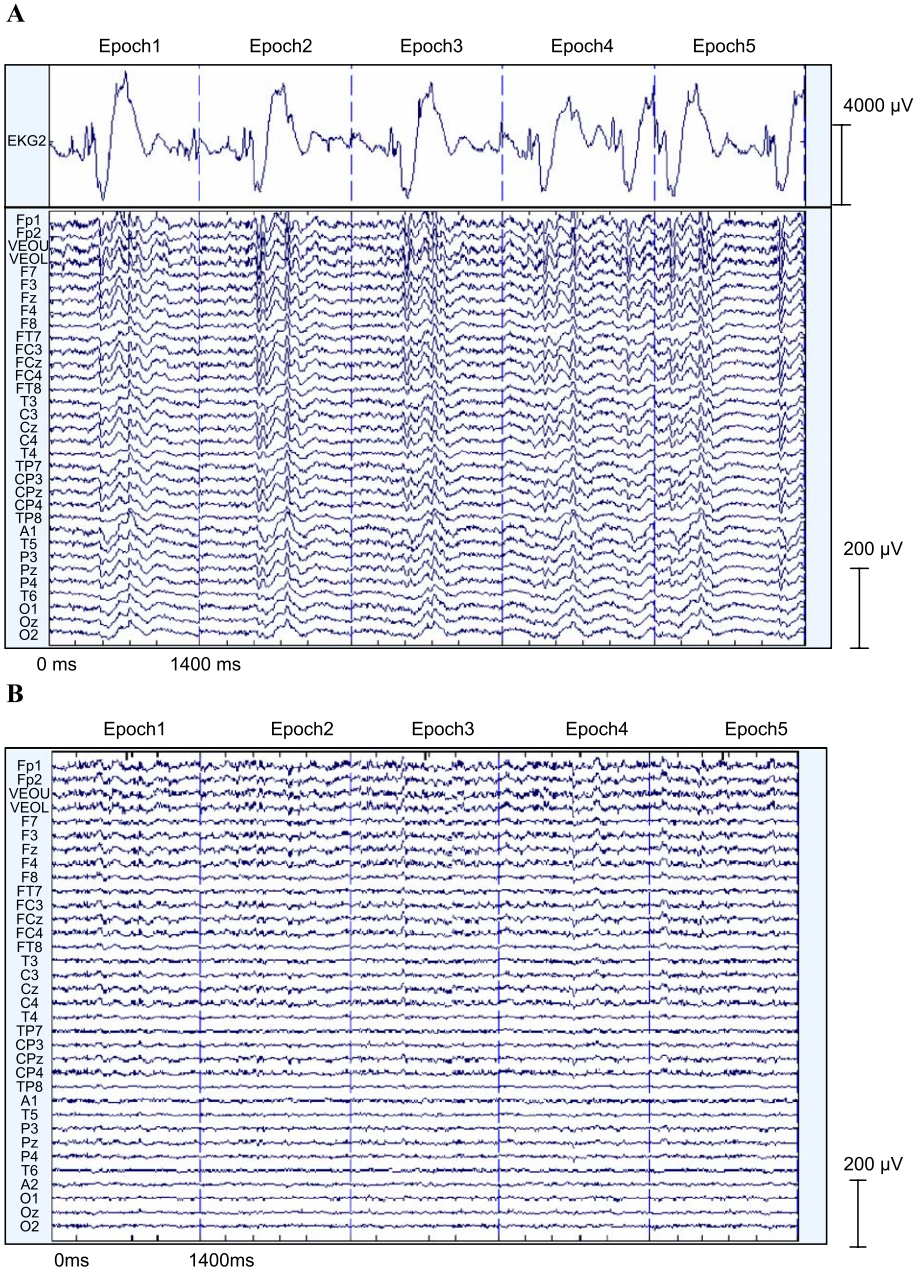

Fig. 2. (A) Raw EEG data (31 channels) along with two eye channels, VEOU and VEOL, and an ECG channel from subject 1. The data is shown here for 5 epochs, each of 1400 ms duration. Each of these gradient-artifact-free epochs was severely contaminated with the BCG artifact. The ECG channel shows the time course of the BCG artifacts. (B) The EEG data after removal of BCG artifacts using ICA.

acquisition software (Acquire 4.3, Neuroscan Inc.). This EEG-fMRI acquisition sequence was repeated 50 times. At the onset of each such acquisition sequence, brief auditory (1000 Hz tones, 250 ms duration) or visual (checkerboard, 250 ms duration) stimuli were presented. Auditory and visual stimuli were presented in two separate runs, referred to here as Run 1 or Run 2, respectively. (Note: Details of auditory and visual stimulus presentation, extraction of event-related potentials and analysis will be presented elsewhere. Here, we focus entirely on removing BCG artifacts from the gradient-artifact-free EEG epochs).

MRI acquisition parameters

Anatomical and functional MRIs acquisitions were performed on a 3-T GE scanner (GE Signa, Milwaukee WI.) using a standard whole head coil. A custom-built head holder was used to prevent head movement. Functional MRI data were acquired using 30 axial slices (4.5 mm thick, 0.5 mm skip, acquisition voxel size: 3.125 × 3.125 × 4.5 mm) parallel to the anterior and posterior commissure covering the whole brain were imaged using a T2* weighted gradient spiral-in and spiral-out pulse sequence (TR = 4000 ms, TE = 30 ms, flip angle = 90° and 1 interleave) (Glover and Lai, 1998, 2001).

EEG recordings

EEG, vertical electro-oculogram (VEOG) and electrocardiogram (ECG) signals were recorded continuously from 36 electrodes using a MRI compatible Quickcap and the Nuamps system (Neuroscan Inc.). VEOG was recorded from two electrodes placed on the infra- and supraorbital ridges of the left eye. ECG was recorded from two electrodes placed just below the left and right collarbone. The signals were bandpass filtered (0.1–70 Hz) and digitized at a rate of 1000 Hz. All leads were referenced to the right mastoid. Electrode impedance was kept below 5 kΩ.

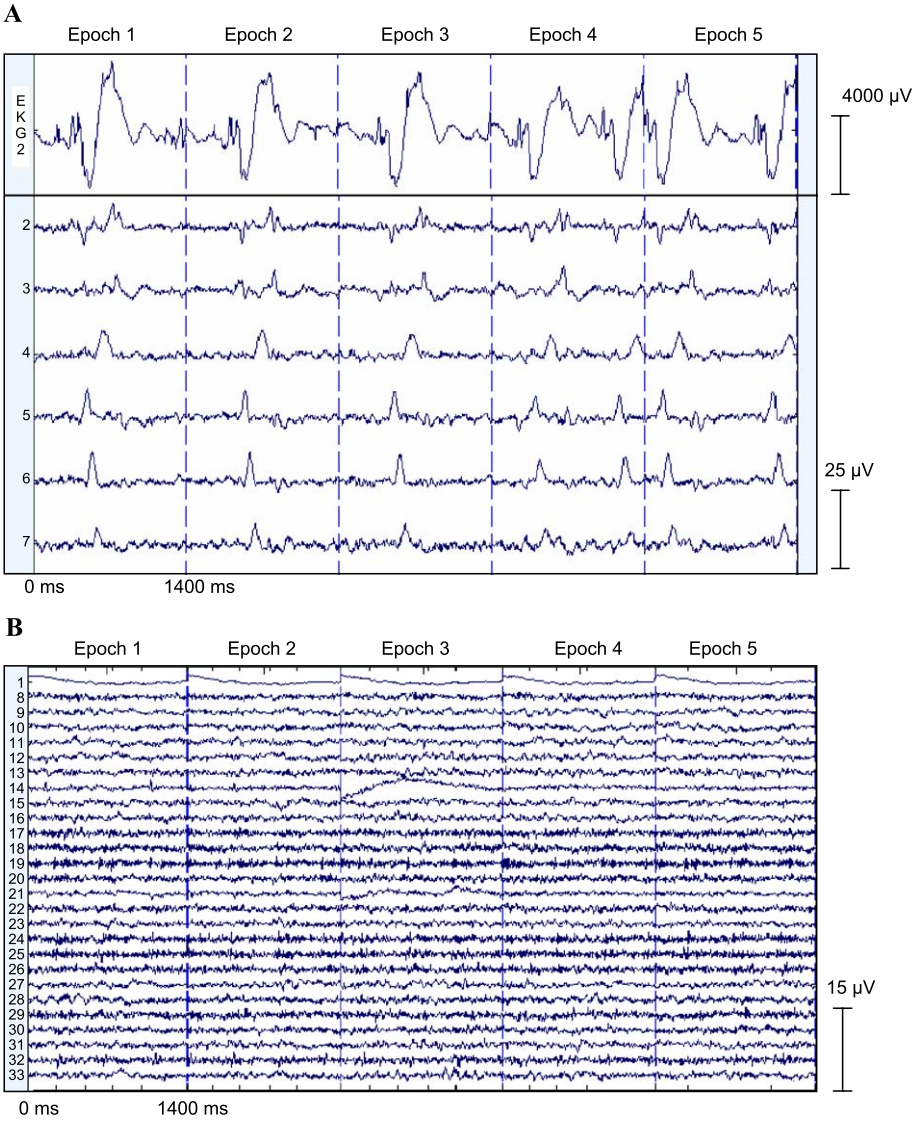

Fig. 3. (A) The ECG signal is shown along ICs 2 to 7 that are clearly identified as the ones with large BCG artifacts. These six components are first removed from the set of 33 ICs, the remaining 27 components (B) were then back-projected into the signal domain to obtain the BCG-artifact-free EEG data shown in Fig. 2B.

EEG data analysis

ICA analysis

EEG data was processed using the Edit 4.3 software (Neuroscan Inc.). ICA was performed using the EEGLAB 4.1 software (Delorme and Makeig, 2004). The EEG data was epoched off-line from −500 to 900 ms relative to the first stimulation and then exported into the EEGLAB 4.1 software. The data set for the ICA consisted of 31 EEG channels and 2 EOG channels. Each data set had 50 epochs each of duration 1.4 s, with 1401 time points. Therefore, each channel had 50 × 1401 = 70050 time points which is much greater than $3N^2$ (= 3 × 33^2 = 2178) points which as a general rule is the minimal number of time points required per channel to find N independent components (Makeig, 2000).

Following ICA, components corresponding to the BCG artifact were identified by visual inspection or by computing correlations with the simultaneously acquired ECG channel. The ECG channel was not included in the ICA analysis because only one of the five subjects had clean ECG data. Correlations were computed between the BCG-related components and the ECG channel for all epochs. Note that the correlations are not computed for morphologically comparing the independent components to the ECG signal as each independent component has large activations that are time locked only to certain specific portions of the artifact. The correlations are done to access which of the components have large activation in the duration of the artifact. Also, the root mean square error (RMSE) was computed between the original ECG channel and the signal obtained by back projecting the selected artifactual components from component-space to the signal-space. We also compared this RMSE with the RMSEs obtained using other sets of randomly selected ICA components. The number of randomly selected ICA components for RMSE calculations was kept the same as the number of suspected BCG-related components. This RMSE comparison was carried out because we believed that the BCG-related components when back-projected into the signal domain should give the minimum RMSE with the ECG signal.

After the ICA analysis, the data were exported back into native Neuroscan format, where it was re-referenced with an average of the A1 and A2 channels for obtaining symmetrical potential distributions. This also helped remove any residual BCG artifacts.

Spectral power comparison before and after BCG artifact removal

In order to evaluate the performance of the ICA method, the power spectra of the data is compared before and after applying the ICA. We have used the Improvement in terms of Normalized Power Spectrum ratio (INPS) (Tong et al., 2001) for demonstrating the suppression of power at BCG-related harmonics. The improvement in terms of INPS is expressed as a ratio of sums of the windowed power of EEG by the formula:

$$INPS = \frac{\sum_{i=1}^{N} P_i^{\text{before\_ICA}}}{\sum_{i=1}^{N} P_i^{\text{after\_ICA}}}$$

where N is the number of harmonics of the ECG and P_i is the spectral power in the 1-Hz frequency window centered at the ith ECG harmonic. In our calculations, we have used $N = 5$, that is, we have considered fundamental ECG frequency (approximately 1.1 Hz) and four harmonics at 2.2, 3.3, 4.4, and 5.5 Hz. The sampling rate of EEG channels was 1000 Hz and we performed a 2048-point FFT for spectral power calculations. The exact window size around each center frequency in the above calculations was $\Delta f = 2 \times \frac{1000}{2048} \approx 0.98$Hz.

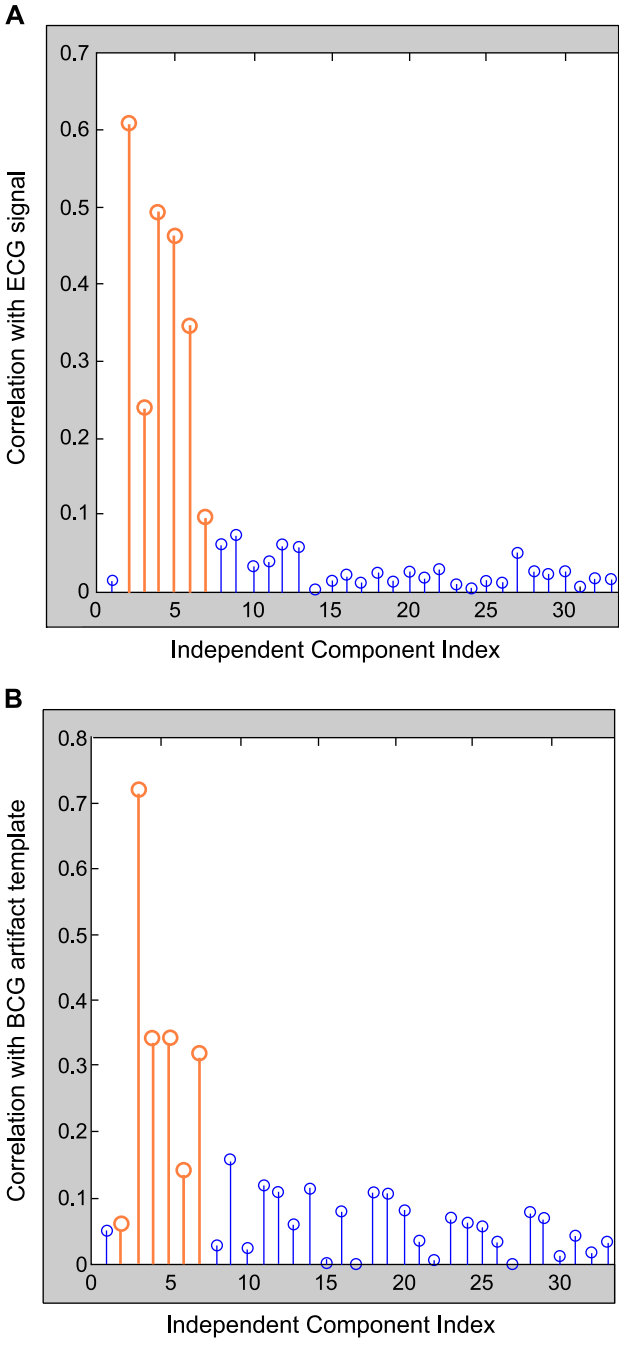

Fig. 4. (A) Correlation of each of the 33 ICs with the ECG signal in subject 1. ICs 2 to 6 show relatively high correlation as compared to other components. Even though IC 7 (as shown in Fig. 3A) does not show a high correlation with the ECG signal, it was marked as artifactual since its morphology follows the periodicity and pattern of ECG signal like ICs 2 to 6. (B) Shows the correlations of the same ICs with the BCG artifact template obtained by averaging over all the EEG channels. In this case, ICs 3 to 7 show high correlation with the BCG template. IC 2 does not show high correlation but it is picked up as BCG artifact related component for the same reason as IC 7 was picked up in the former case.

Table 1
Mean correlation values of the BCG-artifact related ICs and non-BCG-artifact related ICs with BCG artifact template for Runs 1 and 2

Subject no.	Run 1		Run 2	
	Artifact ICs	Non-artifact ICs	Artifact ICs	Non-artifact ICs
1	0.3837	0.0546	0.3983	0.062
2	0.3251	0.0842	0.4182	0.0808
3	0.2953	0.1001	0.3152	0.1066
4	0.1834	0.1229	0.3460	0.1028
5	0.3785	0.0664	0.3391	0.0602

The template is obtained by averaging over all EEG channels.

AAS procedure

To examine the relative performance of our ICA-based procedures, we applied the AAS procedure (Allen et al., 1998) to the same EEG data and compared INPS ratios for ICA versus the AAS. Since good ECG recording was available only in one out of five subjects, we chose not to include ECG channel in the analysis. Instead, all the EEG channels were averaged and the BCG peaks were identified from this averaged waveform. Since the BCG artifact is coherent across all channels and has five to six times larger amplitudes compared to EEG, the averaged waveform is likely to provide an accurate estimate of the BCG artifact peak timings. After we got the peak artifact timings, we created a BCG artifact template for each channel separately by averaging EEG data centered at the peaks of the BCG artifacts and this template was then subtracted from the artifact-corrupted portions of the EEG channel. An R–R interval (Allen et al., 1998), which is a measure of the approximate temporal spread of BCG artifact in the EEG signal of 600 ms centered at the peak of the BCG artifacts, was used for obtaining the artifact template. To have a fair comparison between ICA and AAS, we also incorporated in our AAS procedure the removal of partial BCG artifacts, which did not lie completely in the non-scanning interval. This procedure was performed for all EEG channels individually.

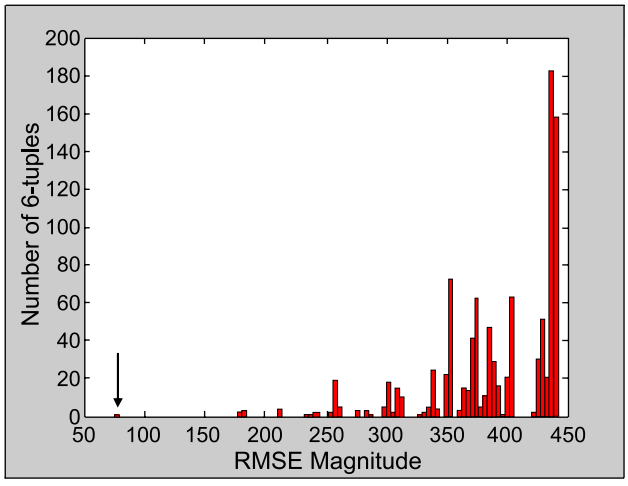

Fig. 5. Results of a boot strapping procedure showing histogram of Root Mean Square Error (RMSE) between the true ECG signal and the one obtained by back-projecting an arbitrary set of 6 ICs into the signal domain. The RMSE corresponding to the 6-tuple identified as artifacts [ICs 2 to 7] is 75.1646 (identified with the arrow), while for the other randomly selected IC 6-tuples, the RMSE lies in the range 350–450. The RMSE of 75.1646 has a probability of occurrence of 0.001 or less, and this RMSE value was also the absolute minimum among the computed RMSEs. Therefore, the 6-tuple with ICs 2–7 accurately represents the BCG artifact.

Results

EEG data before and after removal of BCG artifacts using ICA

We first present an example of the application of ICA for BCG artifact removal based on data from a representative subject (subject 1). As shown in Fig. 2A, the BCG artifacts are prominent

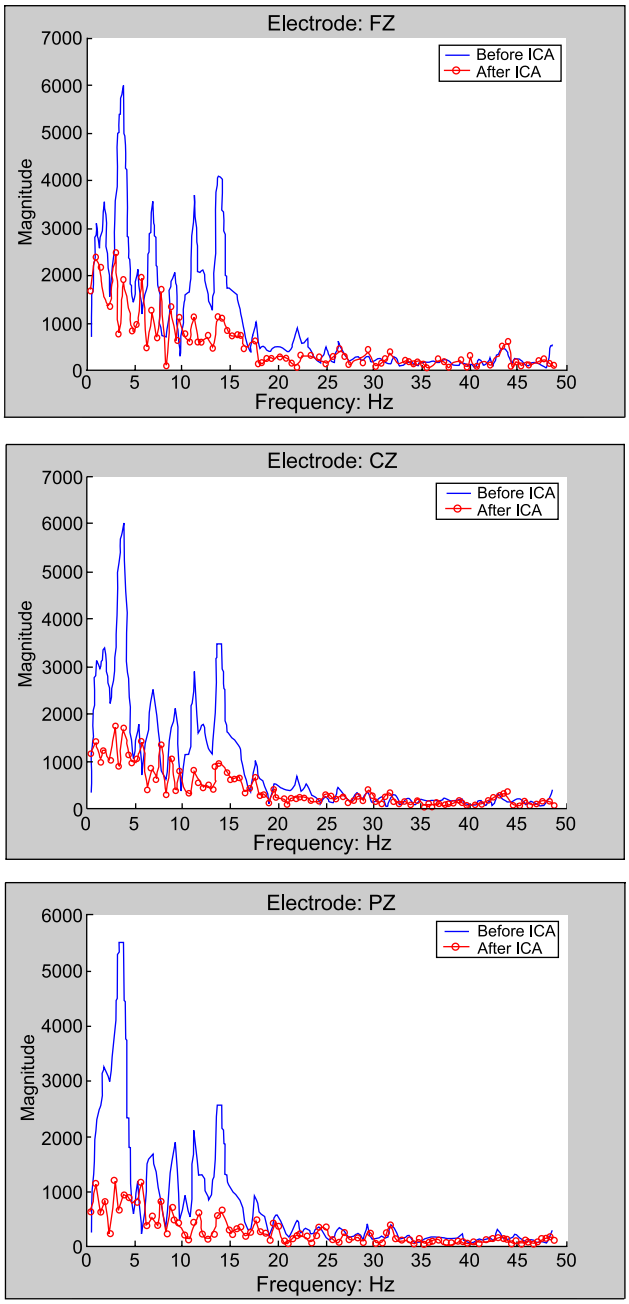

Fig. 6. Comparison of EEG spectra before and after BCG-artifact removal using ICA, at three midline electrodes—FZ, CZ, and PZ. We observed that power in the BCG fundamental frequency (approximately 1.1 Hz) and higher harmonics are significantly reduced.

Table 2A
Spectral power and INPS ratio computation for ICA—Run 1

Subject no.	Power before ICA			Power after ICA			INPS (dB)		
	FZ	CZ	PZ	FZ	CZ	PZ	FZ	CZ	PZ
1	1.65E08	1.65E08	1.58E08	4.85E07	2.60E07	1.22E07	5.3248	8.0255	11.1085
2	3.27E08	9.29E07	8.28E07	1.90E07	2.22E07	6.07E06	12.3502	6.2196	11.3487
3	2.07E08	1.29E08	1.07E08	7.83E07	1.06E07	5.40E07	4.2248	10.8523	2.9791
4	4.42E08	1.22E08	6.39E07	1.95E07	2.03E07	8.71E06	13.5576	7.7794	8.6564
5	7.50E07	5.39E07	4.20E07	1.75E07	1.28E07	5.56E06	6.3122	6.2419	8.7825

in all the epochs and all electrodes. The artifacts are clearly time-locked to the observable peaks in the ECG channel. Fig. 2B shows the same EEG data after removal of BCG artifacts using ICA. Although the ICA analysis was carried out excluding the ECG channels, the BCG artifact has been effectively removed from all the epochs.

BCG-related component identification

Fig. 3 shows the ICs for subject 1, of which ICs 2–7 reveal significant BCG artifacts. Fig. 3A shows ICs 2–7 along with the ECG signal, while Fig. 3B shows the rest of ICs. The components with BCG artifacts can be visually identified as their periodicity and morphology closely follow that of the ECG signal. Correlation analysis between the BCG-related components and ECG channel for all epochs gave high correlation values (Fig. 4A). The correlation of these components with the ECG signal range from approximately 0.25 to 0.62, considerably higher than those for other ICs which are all less than 0.08 (only 15% of the components had correlation values greater than 0.25 while 80% of the ICs had correlation values less than 0.08). Similar findings were observed when the analysis was carried out after replacing reference ECG signal with BCG artifact template obtained by averaging over all EEG channels (Fig. 4B). Most of the BCG artifact related components (ICs 3, 4, 5, 6) were clearly isolated by both the correlation analyses. IC 7 in the first case and IC 2 in the second case show low correlations with the reference signals but still they are chosen as artifactual components because their morphologies follow the periodicity and pattern of ECG signal like ICs 3 to 6. Table 1 summarizes the correlation analysis data between BCG artifact template and artifactual and non artifactual ICs. It shows the mean correlation values between the artifact template and artifactual and non-artifactual ICs for the five subjects. For both Runs 1 and 2, the mean correlation of the BCG-artifact related ICs with the artifact template is significantly higher than the non BCG-artifact related ICs (Wilcoxon Sign Ranked test; $Z = 2.022$, $P < 0.05$). In order to further validate the choice of these ICs as ones that were artifact related, we used a boot strapping procedure which examined the Root Mean Square Error (RMSE) between the true ECG signal and the one obtained by back-projecting an arbitrary set of 6 ICs into the signal domain. Fig. 5 shows, for subject 1, the RMSEs between the ECG signal and the back-projections of randomly selected N-tuples of ICs to the signal space. It was observed that the RMSE corresponding to the 6 BCG-related artifact components (ICs 2 to 7) is much less as compared to RMSE for any other combination of six components. Moreover, the RMSE corresponding to the six chosen ICs was found to have a probability of occurrence of 0.001 or less, and this RMSE value was also the absolute minimum among the computed RMSEs. This provides further validation that the ICs chosen as being BCG-artifact-related represent the artifact optimally and hence are the best candidates for removal. Similar results were obtained for subjects 2–5.

We further computed the kurtosis to verify the non-Gaussianity of independent components. The kurtosis data of the derived components is presented in Table 4 for Runs 1 and 2. The median kurtosis of the ICs for the five subjects lies in the range of approximately 4–9. Therefore in each case, the ICs are non-Gaussian since a Gaussian distribution has zero kurtosis.

Spectral power before and after BCG-artifact removal

Spectral power in ECG harmonic frequencies was computed for each subject before and after ICA, from which INPS rations were then derived. Three midline electrodes were examined: FZ, CZ, and PZ for all the five subjects. Fig. 6 shows the power spectra of raw EEG data before and after ICA. The marked reduction in the ECG harmonic power suggests that the contribution of these peaks has been effectively suppressed from the EEG data. As is evident from the figures, the power in the higher frequencies is approximately unchanged. Tables 2A and B show the INPS ratios (in dB) at the three electrodes for five subjects for both Runs 1 and 2. In each case, it is evident that significant reductions were obtained in ECG harmonic spectral power as a result of applying ICA. Averaging over the five subjects, a reduction of 8.35, 7.82, 8.575 dB was achieved at FZ, CZ, and PZ electrodes respectively

Table 2B
Spectral power and INPS ratio computation for ICA—Run 2

Subject no.	Power before ICA			Power after ICA			INPS (dB)		
	FZ	CZ	PZ	FZ	CZ	PZ	FZ	CZ	PZ
1	2.91E08	1.93E08	1.56E08	4.79E07	2.39E07	1.35E07	7.845	9.0598	10.6344
2	2.92E08	1.71E08	8.05E07	1.95E07	5.80E07	9.55E06	11.7629	4.6842	9.2566
3	3.61E08	2.04E08	1.30E08	1.45E08	1.65E08	1.00E08	3.9579	0.9144	1.1059
4	4.37E08	1.50E08	6.23E07	3.91E07	2.36E07	8.02E06	10.4865	8.0491	8.9037
5	9.40E07	8.64E07	9.41E07	7.06E06	1.21E07	1.96E07	11.2448	8.5395	6.8159

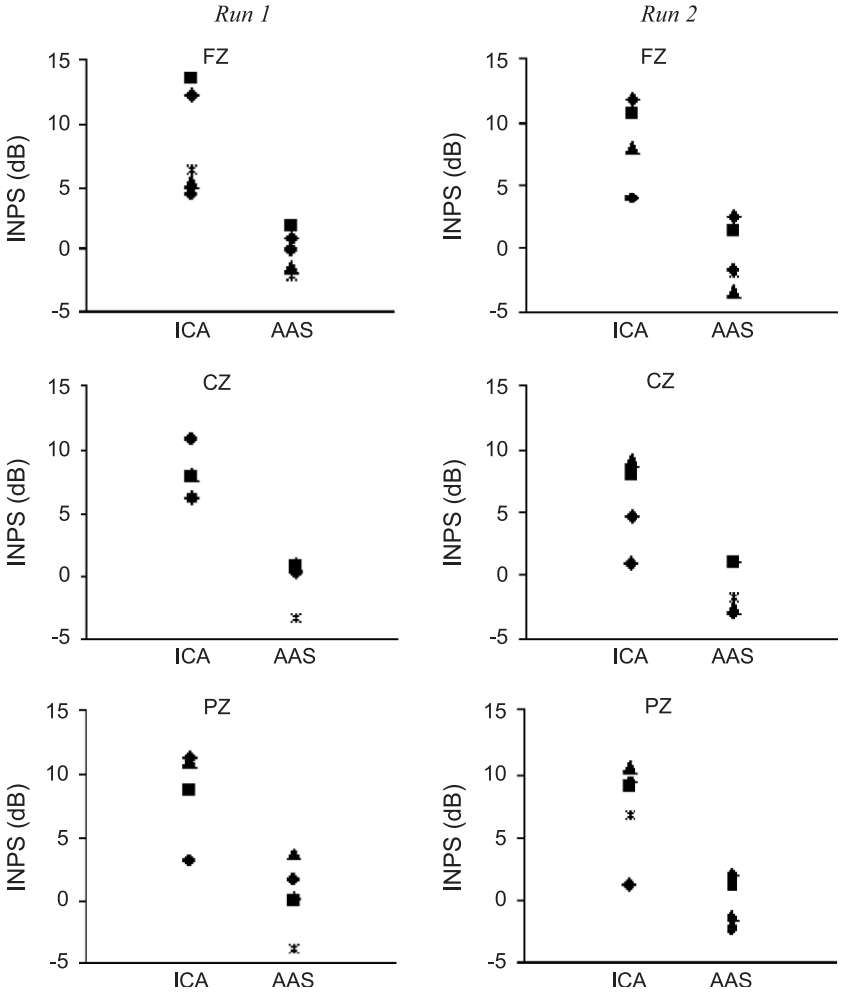

Fig. 7. Comparison of reduction in power in the BCG fundamental frequency (~ 1.1 Hz) and higher harmonics between ICA- and AAS-based procedures, as indexed by INPS ratios. Results are shown for all 5 subjects using data from three midline electrodes FZ, CZ, and PZ, for both Runs 1 and 2. INPS ratios for ICA-based BCG artifact reduction procedures were much higher than those for the AAS procedure.

for Run 1 and 9.06, 6.25, and 7.34 dB was achieved for Run 2. For both Runs 1 and 2, these reductions were statistically significant (Wilcoxon Sign Rank test; $Z > 2.0$, $P < 0.05$).

Comparison with the AAS procedure

Fig. 7 compares the performance of ICA- and AAS-based procedures, in terms of INPS ratios which are plotted for the three electrodes (FZ, CZ, PZ) for Runs 1, 2, and for all five subjects. These ratios are also summarized in Tables 2A, 2B and 3A, 3B for Runs 1 and 2. Averaging over the five subjects, the AAS procedure results in a reduction of −0.33, −0.27, 0.24 dB at FZ, CZ, and PZ electrodes for Run 1 and −0.69, −1.08 and −0.58 dB for Run 2. Comparing these reductions with those obtained with ICA, we found that ICA performs significantly better than AAS (Wilcoxon Sign Rank test; $Z > 2.0$, $P < 0.05$).

Discussion

In this report, we have described new ICA-based procedures for removing BCG artifacts from EEG recorded inside an MRI scanner. ICA decomposition allowed us to identify and remove BCG artifacts in a reliable manner. ICA procedures were efficient

Table 3A
Spectral power and INPS ratio computation for AAS procedure—Run 1

Subject no.	Power before AAS			Power after AAS			INPS (dB)		
	FZ	CZ	PZ	FZ	CZ	PZ	FZ	CZ	PZ
1	1.65E + 08	1.65E08	1.58E08	2.41E08	1.36E08	7.00E07	−1.6322	0.8378	3.5253
2	3.27E + 08	9.29E07	8.28E07	2.74E08	8.66E07	8.27E07	0.7572	0.3079	0.005
3	2.07E + 08	1.29E + 08	1.07E + 08	2.16E08	1.23E08	7.51E07	−0.1802	0.21	1.548
4	4.42E + 08	1.22E08	6.39E07	3.01E08	1.02E08	6.42E07	1.6654	0.7754	−0.0194
5	7.50E + 07	5.39E07	4.20E07	1.26E08	1.20E08	1.03E08	−2.2485	−3.4898	−3.872

Table 3B
Spectral power and INPS ratio computation for AAS procedure—Run 2

Subject no.	Power before AAS			Power after AAS			INPS (dB)		
	FZ	CZ	PZ	FZ	CZ	PZ	FZ	CZ	PZ
1	2.91E08	1.93E08	1.56E08	6.48E08	3.58E08	2.12E08	−3.469	−2.6911	−1.3381
2	2.92E08	1.71E08	8.05E07	1.69E08	1.33E08	5.33E07	2.3852	1.076	1.7871
3	3.61E + 08	2.04E + 08	1.30E + 08	5.52E08	4.18E08	2.29E08	−1.8431	−3.1255	−2.4688
4	4.37E08	1.50E08	6.23E07	3.16E08	1.17E08	4.97E07	1.4042	1.0939	0.9837
5	9.40E07	8.64E07	9.41E07	1.47E08	1.30E08	1.44E08	−1.9386	−1.763	−1.8501

in reducing spectral power in the fundamental ECG frequency and its higher harmonics at all the scalp electrodes. Detailed quantitative comparisons showed that ICA-based procedures performed significantly better than more standard techniques that involve AAS. One additional advantage of the ICA-based procedure is that it does not require a reference channel for isolating the artifacts.

ICA is an obvious choice for removing BCG artifacts as it has been used successfully in removing various artifacts from EEG recordings with negligible loss of neural signals of interest (Iriarte et al., 2003; Jung et al., 2000a,b; Makeig et al., 1997; Tong et al., 2001). In terms of component identification, the overall strategy used was similar to Jung et al. (2000a,b) study pertaining to removal of eye activity artifacts from visual event-related potentials in normal and clinical subjects.

The BCG artifacts in ICA components were so prominent that in most cases these artifacts could be identified by visual inspection. In most cases, five to six components with BCG artifacts could be clearly recognized and these components were eliminated from the set of ICs. BCG artifact-free EEG data were then reconstructed by back-projecting the remaining components into the original signal space. Previous studies that have used ICA for artifact removal in EEG data have used both spatial and temporal information to isolate ICs with artifacts. For example, ocular artifact can be immediately recognized by its spatial map which shows focal activity in periocular and anterior frontal sites and the time course of the corresponding IC gives a very high correlation with, and also visually resembles, eye-blink activity on the VEOG electrodes (Jung et al., 2000a,b). ICs containing BCG artifacts are somewhat different in the sense that even though they too are caused by a physiological process independent of electrical brain activity, the spatial maps for such components are more diffuse and global because of the greater physical separation of heart from brain regions. But it was on the basis of their time courses, which have striking similarity with the ECG channel in terms of temporal location, rate, and duration of peaks that they could be easily identified visually. Additional means of identification is typically carried out by correlating the components corresponding to BCG artifacts with either a simultaneously recorded ECG channel, or an estimate of the BCG artifact obtained by averaging the epochs of all the EEG channels. This estimation by averaging is based on the assumption that due to the physical separation between the heart and brain regions, all the EEG channels are approximately equally affected by the BCG artifact.

The main assumptions that underlie ICA decomposition of EEG time series are (1) EEG data recorded at multiple scalp sensors are linear sums of temporally independent components, (2) the ICs arise from spatially fixed distinct or overlapping brain or extra-brain sources, and (3) statistical distributions of the ICs are non-Gaussian (Jung et al., 2000a,b; Makeig et al., 1997). As Tong et al. (2001) point out, results of ICA are only as good as the fit of the data to the ICA assumptions, primarily independence and spatial stability of the underlying sources. In the case of BCG artifacts, the artifact magnitude and temporal location depend linearly on the amplitude and timing of ECG signal (a process that is physiologically independent from neural activity) and the artifact closely follows the periodicity and morphology of the ECG signal. Therefore, the assumption of temporal independence and linear mixing of BCG artifacts to the EEG data is satisfied. The second assumption about spatial stability is also satisfied since most of the artifacts arise from small movements in the magnet, predominantly from the head moving. The cardiac pulsatility generates only tiny motions, such that the electrode and wire positions are approximately stationary on average over the cardiac cycle. Also, the swelling of the brain during the cardiac cycle is approximately stationary on average. The assumption regarding the non-Gaussianity of the ICs is corroborated by the kurtosis data provided in Table 4. The median kurtosis of the ICA components for the five subjects lies in the range of approximately 4 to 9. Because the kurtosis for a Gaussian distribution is 0, this points to the fact that ICA component activations have non-Gaussian distributions.

Our ICA-based procedures performed significantly better than an AAS procedure such as the one described by Allen et al. (1998). Reductions in artifact levels as indexed by the INPS ratio were significantly greater with the ICA-based method compared to the AAS procedure. For most of the subjects and both runs, the INPS ratios for ICA-based procedures ranged from 6 to 10 dB, while the INPS ratios obtained for AAS procedure had values close to 0. Our analysis also uncovered potential problems with the AAS procedure—in some cases, the INPS values were negative, pointing to the fact that ECG spectral power in the corrected EEG data was greater than the ECG spectral power before the correction. This degraded performance results from the errors in precise determination of ECG peaks during the simultaneous EEG/fMRI acquisition. In AAS procedure, the ECG peaks are used to locate the positions of BCG artifacts in the EEG signals, which have to be averaged to obtain the BCG artifact template. In a 3-T scanner, the ECG signal is also

Table 4
Median kurtosis of ICA components for Runs 1 and 2

Subject no.	Median kurtosis of ICA components	
	Run 1	Run 2
1	3.9013	8.4317
2	8.6016	8.9887
3	7.8354	6.2023
4	5.9196	6.6975
5	3.9103	4.2208

distorted and therefore it is difficult to precisely determine the ECG peak positions by automated methods. In contrast, the proposed ICA-based methods represent efficient and automated procedures for BCG artifact removal.

The problem of AAS-based procedures is further confounded in interleaved EEG/fMRI acquisitions where short gradient-artifact-free EEG epochs rather than continuous EEG recordings tend to be available. In this case, averaging has to be done over BCG artifacts which may be separated considerably in time and so the problem of non-stationarities in the ECG lead to further errors in the estimation of the artifact template. Our ICA-based procedures again prove advantageous because short EEG epochs can be easily used for BCG artifact removal without any violation of the assumptions of the ICA procedures. Thus, in our study, all the gradient-artifact-free EEG epochs are concatenated to form a single time series for each EEG channel and these data were provided as input to the ICA decomposition algorithm.

Bonmassar et al. (1999) have presented two different techniques for removing the BCG artifact. The first technique uses a spatial filter and takes advantage of the fact that the BCG artifact tends to be more diffuse spatially than the neural signals of interest. This technique makes use of large number of EEG channels (typically 64 or 128) to derive a spatial filter which essentially projects multiple channel signals into a one-dimensional space that follows the direction of maximum signal-to-noise ratio. The second technique (Bonmassar et al., 2002) uses adaptive filtering and takes advantage of temporal information alone to remove artifacts, treating each of the EEG channels independently. The advantage of using ICA for eliminating the BCG artifact is that it uses both spatial as well as temporal information simultaneously for deriving the components and hence the components reflect the independent activity from distinct sources present at different or overlapping spatial locations (Kobayashi et al., 1999; van Hateren, 1993; van Hateren and Ruderman, 1998; van Hateren and van der Schaaf, 1998). The spatial information is embedded in the correlations between neighboring electrodes on the scalp and the temporal information is embedded in the EEG time series recorded at each of the electrodes. Since ICA uses all the EEG channels simultaneously to come up with maximally statistically independent time courses of activations and their associated spatial maps, both the temporal and spatial information is used effectively at the same time. A further advantage of the ICA-based procedure is that whereas the spatial filtering method (Bonmassar et al., 1999) also needs data collected outside the scanner for estimating a noise covariance matrix (used for maximizing the signal-to-noise ratio), ICA is a completely self-contained procedure which can be used without requiring any additional data.

An additional advantage of the ICA approach is that it does not require the ECG channel during the analysis to derive the components, unlike the adaptive filtering approach which needs the ECG or other related motion channels to derive the adaptive filter. The fact that BCG artifact independently and linearly mixes with neural signal generators and other artifact sources to give the scalp EEG recordings is sufficient for ICA to isolate the BCG-related components from the data. While employing ICA technique, ECG signals may or may not be included in the analysis. If the ECG signal is included, then some components will represent the heart-related BCG activity and will form the best candidates for removal in order to get rid of the BCG artifact. The advantage of using ICA is that even if ECG signal is not available for recording or gets severely distorted during recording, ICA will still give components representing the ballistocardiogram activity because the generator of this activity, that is, the cardiac pulsation is physiologically (and statistically) independent from the EEG activity of the neurophysiological sources. The only possible reason for recording an ECG signal might be to improve the detection of artifactual ICs.

At present, the artifact-related components are obtained through a combination of objective measures like correlation with the ECG channel and subjective judgment based on visually examination of the morphology and time course of the IC waveforms. Future studies will investigate more automated ways of detecting BCG artifacts. Also, applications of ICA to remove gradient artifacts will be explored so that event-related potentials can be extracted robustly during continuous EEG/fMRI acquisition.

Acknowledgments

This research was supported by a grant from the Bio-X interdisciplinary initiative program at Stanford University and by a grant from the NIH (HD40761) and grant (NIH RRP4109784). We would like to thank A. Delorme and S. Makeig of Swartz Center for Computational Neuroscience, UCSD for making the EEGLAB software available for analysis.

References

Ahlfors, S.P., Simpson, G.V., Dale, A.M., Belliveau, J.W., Liu, A.K., Korvenoja, A., Virtanen, J., Huotilainen, M., Tootell, R.B., Aronen, H.J., Ilmoniemi, R.J., 1999. Spatiotemporal activity of a cortical network for processing visual motion revealed by MEG and fMRI. J. Neurophysiol. 82 (5), 2545–2555.

Allen, P.J., Polizzi, G., Krakow, K., Fish, D.R., Lemieux, L., 1998. Identification of EEG events in the MR scanner: the problem of pulse artifact and a method for its subtraction. NeuroImage 8 (3), 229–239.

Babiloni, F., Carducci, F., Cincotti, F., Del Gratta, C., Roberti, G.M., Romani, G.L., Rossini, P.M., Babiloni, C., 2000a. Integration of high resolution EEG and functional magnetic resonance in the study of human movement-related potentials. Methods Inf. Med. 39 (2), 179–182.

Babiloni, F., Carducci, F., Del Gratta, C., Roberti, G.M., Cincotti, F., Bagni, O., Romani, G.L., Rossini, P.M., Babiloni, C., 2000b. Multimodal integration of high resolution EEG, MEG and functional magnetic resonance data. Int. J. Bioelectromagn. 1 (1).

Bell, A.J., Sejnowski, T.J., 1995. An information-maximization approach to blind separation and blind deconvolution. Neural Comput. 7 (6), 1129–1159.

Bonmassar, G., Anami, K., Ives, J., Belliveau, J.W., 1999. Visual evoked potential (VEP) measured by simultaneous 64-channel EEG and 3T fMRI. NeuroReport 10 (9), 1893–1897.

Bonmassar, G., Hadjikhani, N., Ives, J.R., Hinton, D., Belliveau, J.W., 2001. Influence of EEG electrodes on the BOLD fMRI signal. Hum. Brain Mapp. 14 (2), 108–115.

Bonmassar, G., Purdon, P.L., Jaaskelainen, I.P., Chiappa, K., Solo, V., Brown, E.N., Belliveau, J.W., 2002. Motion and ballistocardiogram artifact removal for interleaved recording of EEG and EPs during MRI. NeuroImage 16 (4), 1127–1141.

Comon, P., 1994. Independent component analysis: a new concept ? Signal Process., Elsevier 36 (3), 287–314.

Dale, A.M., Liu, A.K., Fischl, B.R., Buckner, R.L., Belliveau, J.W., Lewine, J.D., Halgren, E., 2000. Dynamic statistical parametric mapping: combining fMRI and MEG for high-resolution imaging of cortical activity. Neuron 26 (1), 55–67.

Delorme, A., Makeig, S., 2004. EEGLAB: an open source toolbox for analysis of single-trial EEG dynamics including independent component analysis. J. Neurosci. Methods 134 (1), 9–21.

George, J.S., Aine, C.J., Mosher, J.C., Schmidt, D.M., Ranken, D.M., Schlitt, H.A., Wood, C.C., Lewine, J.D., Sanders, J.A., Belliveau, J.W., 1995. Mapping function in the human brain with magnetoencephalography, anatomical magnetic resonance imaging, and functional magnetic resonance imaging. J. Clin. Neurophysiol. 12 (5), 406–431.

Glover, G.H., Lai, S., 1998. Self-navigated spiral fMRI: interleaved versus single-shot. Magn. Reson. Med. 39 (3), 361–368.

Glover, G.H., Law, C.S., 2001. Spiral-in/out BOLD fMRI for increased SNR and reduced susceptibility artifacts. Magn. Reson. Med. 46 (3), 515–522.

Goldman, R.I., Stern, J.M., Engel Jr., J., Cohen, M.S., 2000. Acquiring simultaneous EEG and functional MRI. Clin. Neurophysiol. 111 (11), 1974–1980.

Hyvarinen, A., Karhunen, J., Oja, E., 2001. Independent Component Analysis. John Wiley and Sons.

Iriarte, J., Urrestarazu, E., Valencia, M., Alegre, M., Malanda, A., Viteri, C., Artieda, J., 2003. Independent component analysis as a tool to eliminate artifacts in EEG: a quantitative study. J. Clin. Neurophysiol. 20 (4), 249–257.

Jung, T.P., Makeig, S., Humphries, C., Lee, T.W., McKeown, M.J., Iragui, V., Sejnowski, T.J., 2000a. Removing electroencephalographic artifacts by blind source separation. Psychophysiology 37 (2), 163–178.

Jung, T.P., Makeig, S., Westerfield, M., Townsend, J., Courchesne, E., Sejnowski, T.J., 2000b. Removal of eye activity artifacts from visual event-related potentials in normal and clinical subjects. Clin. Neurophysiol. 111 (10), 1745–1758.

Jung, T.P., Makeig, S., McKeown, M.J., Bell, A.J., Lee, T.W., Sejnowski, T.J., 2001a. Imaging brain dynamics using independent component analysis. Paper Presented at the Proceedings of the IEEE. July.

Jung, T.P., Makeig, S., Westerfield, M., Townsend, J., Courchesne, E., Sejnowski, T.J., 2001b. Analysis and visualization of single-trial event-related potentials. Hum. Brain Mapp. 14 (3), 166–185.

Kobayashi, K., James, C.J., Nakahori, T., Akiyama, T., Gotman, J., 1999. Isolation of epileptiform discharges from unaveraged EEG by independent component analysis. Clin. Neurophysiol. 110 (10), 1755–1763.

Krakow, K., Allen, P.J., Symms, M.R., Lemieux, L., Josephs, O., Fish, D.R., 2000. EEG recording during fMRI experiments: image quality. Hum. Brain Mapp. 10 (1), 10–15.

Lee, T.W., Girolami, M., Sejnowski, T.J., 1999. Independent component analysis using an extended infomax algorithm for mixed subgaussian and supergaussian sources. Neural Comput. 11 (2), 417–441.

Lemieux, L., Salek-Haddadi, A., Josephs, O., Allen, P., Toms, N., Scott, C., Krakow, K., Turner, R., Fish, D.R., 2001. Event-related fMRI with simultaneous and continuous EEG: description of the method and initial case report. NeuroImage 14 (3), 780–787.

Liebenthal, E., Ellingson, M.L., Spanaki, M.V., Prieto, T.E., Ropella, K.M., Binder, J.R., 2003. Simultaneous ERP and fMRI of the auditory cortex in a passive oddball paradigm. NeuroImage 19 (4), 1395–1404.

Makeig, S., 2000. Frequently Asked Questions about ICA applied to EEG and MEG data (Cartographer).

Makeig, S., Jung, T.P., Bell, A.J., Ghahremani, D., Sejnowski, T.J., 1997. Blind separation of auditory event-related brain responses into independent components. Proc. Natl. Acad. Sci. U. S. A. 94 (20), 10979–10984.

Menon, V., Ford, J.M., Lim, K.O., Glover, G.H., Pfefferbaum, A., 1997. Combined event-related fMRI and EEG evidence for temporal–parietal cortex activation during target detection. NeuroReport 8 (14), 3029–3037.

Salek-Haddadi, A., Merschhemke, M., Lemieux, L., Fish, D.R., 2002. Simultaneous EEG-correlated ictal fMRI. NeuroImage 16 (1), 32–40.

Sijbers, J., Van Audekerke, J., Verhoye, M., Van der Linden, A., Van Dyck, D., 2000. Reduction of ECG and gradient related artifacts in simultaneously recorded human EEG/MRI data. Magn. Reson. Imaging 18 (7), 881–886.

Tong, S., Bezerianos, A., Paul, J., Zhu, Y., Thakor, N., 2001. Removal of ECG interference from the EEG recordings in small animals using independent component analysis. J. Neurosci. Methods 108 (1), 11–17.

van Hateren, J.H., 1993. Spatial, temporal and spectral pre-processing for colour vision. Proc. R. Soc. London, B Biol. Sci. 251 (1330), 61–68.

van Hateren, J.H., Ruderman, D.L., 1998. Independent component analysis of natural image sequences yields spatio-temporal filters similar to simple cells in primary visual cortex. Proc. R. Soc. London, B Biol. Sci. 265 (1412), 2315–2320.

van Hateren, J.H., van der Schaaf, A., 1998. Independent component filters of natural images compared with simple cells in primary visual cortex. Proc. R. Soc. London, B Biol. Sci. 265 (1394), 359–366.

Woldorff, M.G., Matzke, M., Zamarripa, F., Fox, P.T., 1999. Hemodynamic and electrophysiological study of the role of the anterior cingulate in target-related processing and selection for action. Hum. Brain Mapp. 8 (2–3), 121–127.